ELSEVIER

Journal of Alloys and Compounds 235 (1996) 201–209

Journal of ALLOYS AND COMPOUNDS

X-ray single crystal refinements on some RT_2Ge_2 compounds (R = Ca, Y, La, Nd, U; T = Mn–Cu, Ru–Pd): evolution of the chemical bonds

G. Venturini, B. Malaman

Laboratoire de Chimie du Solide Minéral, Université Henri Poincaré-Nancy I, associé au CNRS (URA 158), B.P. 239, 54506 Vandoeuvre les Nancy Cedex, France

Received 8 October 1995

Abstract

We report on single crystal refinement of 22 $ThCr_2Si_2$-type structure germanides of composition RT_2Ge_2 (R = Ca, Y, La, Nd, U; T = Mn, Fe, Co, Ni, Cu, Ru, Rh, Pd). The interatomic distances and their variations with R size, R valency and the position of the transition metal in the Periodic Table are analysed from 35 refined structures. The T–Ge bond is always strong except in the Mn compounds. The Ge–Ge bond is stronger in the right-hand side transition metal compounds. This effect is discussed in term of a previous theoretical work. Among the other contacts T–T, R–T and R–R, the T–T contacts seem to play an important role in the Ru and Rh compounds, whereas it is believed that the R–T contacts control the cell dimensions of Fe and Co compounds. This paper examines the relationships between the interatomic distances and the magnetic behaviour of manganese $ThCr_2Si_2$-type structure compounds.

Keywords: Ternary germanides; Chemical bonding; Magnetic behaviour; X-ray structure; $ThCr_2Si_2$-type structure

1. Introduction

The $ThCr_2Si_2$-type structure [1] is one of the most frequently observed structures in ternary rare earth compounds. During the last few decades, quite a number of physical studies have been devoted to the isotypic silicides and germanides [2]. During our research on the ternary silicides and germanides RMn_2Si_2 and RMn_2Ge_2 (R = Ca or lanthanides), we discovered an unusual magnetic behaviour of the (001) Mn planes [3,4]. The calcium and lightest rare earth compounds, i.e. compounds characterized by the largest Mn–Mn and Mn–Si(Ge) distances, are characterized by antiferromagnetic (001) Mn planes. The ferromagnetic transition, previously measured in these compounds [2], is in fact a second magnetic transition arising from the canting of the Mn moments in the (001) plane.

In order to obtain more precision on this behaviour, several solid solutions of composition $RMn_{2-x}T_xGe_2$ (R = Ca, La, Nd; T = Fe, Cu) have been studied. It was then observed that the substitution of manganese by iron in $LaMn_2Ge_2$ provokes a considerable decrease in the ferromagnetic transition temperature [5] while the decrease of T_c through substitution of Mn by Cu seems to be less dramatic [6]. Contrary to these results, substitution of manganese by iron in $CaMn_2Ge_2$ enhances the ferromagnetic character [7].

These effects may arise from deviations, although slight, of the interatomic distances. It was thus planned to investigate them using X-ray single crystal refinements. A similar study, mainly devoted to the 4d metals, was previously undertaken for RT_2Ge_2 compounds (R = Y, Ca, Nd; T = Mn, Cu, Ru, Rh, Pd) [8]. In order to determine the evolution of the chemical bond throughout the whole series of $ThCr_2Si_2$-type structure germanides, it was necessary to perform X-ray single crystal analysis on the remaining 3d series (T = Fe, Co, Ni) compounds and to complete the study with corresponding lanthanum and/or calcium compounds.

2. Experimental

Samples were prepared from stoichiometric amounts of pure elements. After a first reaction in a silica tube under argon, the mixture was melted in an

SSDI 0925-8388(95)02140-X

induction furnace. Single crystals were extracted from the solidified ingots and mounted on an automatic diffractometer Nonius CAD4F (Mo Kα). Data was recorded in the 3–35° θ range. The z_{Ge} parameter and the isotropic thermal factors were refined using the SHELX procedure [9]. Absorption has been neglected ($\mu R < 1$).

3. Results

The crystallographic data and refined parameters are gathered in Table 1. For a given T metal, the z_{Ge} parameter systematically decreases with increase of rare earth size. Within standard errors, our refinements lead to identical z_{Ge} values as those obtained for previously studied calcium compounds CaT_2Ge_2 (T = Mn, Co, Ni, Cu) [10,11] (except for $CaMn_2Ge_2$ (0.3835(1) compared with 0.381).

The principle interatomic distances of the rare earth compounds are presented in Table 2. Table 3 gives the interatomic distances for calcium and uranium compounds. For comparison sake, the interatomic distances for Nd and Y compounds are also given. Table 4 gives the interatomic distances for the $LaMn_{2-x}Fe_xGe_2$, $LaMn_{2-x}Cu_xGe_2$ and $CaMn_{2-x}Fe_xGe_2$ solid solutions.

4. Analysis of the results

4.1. Structure description

The $ThCr_2Si_2$ structure type of RT_2X_2 stoichiometry compounds may be described as constituted of square atomic planes, stacked along the c axis according to the sequence R–X–T_2–X–R. The T layers are twice as densely populated as the other R and X layers.

A description based on the coordination polyhedra would locate the transition metal T in a tetrahedral site of X atoms (Fig. 1(a)). The large R metal would, in an identical manner, be located in a 16-fold coordination polyhedron, the dimensions of which are defined by the X–X and T–X contacts (Fig. 1(b)). This would yield 8X and 8T nearest neighbours, each element building a quadratic prism around R. The X element is located in a quadratic antiprism [T_4X_4] (Figs. 1(c) and 2). The dimensions of this antiprism are directly related to the cell parameters with the height of the X atom defined by the free parameter z_X.

In order to accommodate the six possible interatomic contacts T–X, X–X, R–X, R–T, T–T and R–R, the structure uses its three adjustable parameters a, c and z_X. Relative dilatations of the interatomic distances from atomic radii [12], ($\Delta[i-j] = (d_{ij} - \Sigma r_i)/\Sigma r_i$), given in Table 2, seem to suggest three main interatomic contacts: X–X, R–X and T–X. The corresponding distances are given by the following equations:

$$d_{X-X} = 2l \tag{1}$$

$$d_{R-X} = (l^2 + a^2/2)^{1/2} \tag{2}$$

$$d_{T-X} = ([h-l]^2 + a^2/4)^{1/2} \tag{3}$$

Where a, h, l refer to Fig. 2. Assuming that $d_{R-X} < (d_{X-X}^2/4 + 2d_{T-X}^2)^{1/2}$, the system leads to the solutions:

$$c = 4h = 2d_{X-X} + 2(d_{X-X}^2/2 - 2d_{R-X}^2 + 4d_{T-X}^2)^{1/2} \tag{4}$$

$$a = (2d_{R-X}^2 - d_{X-X}^2/2)^{1/2} \tag{5}$$

$$z_X = 1/2 - d_{X-X}/2c \tag{6}$$

This in turn signifies that, with d_{X-X} and d_{T-X} constant, the increase in size of the rare earth element should induce a decrease of the c parameter. This result would suggest a negative variation of the c parameter as correlated to strong X–X contacts.

On the contrary, the absence of X–X bonds allows free variation of the parameter c to accommodate the R–X contacts; the parameter a may be kept constant yielding unchanged T–X and T–T contacts. This situation is encountered in the RRu_2P_2 series [13,14].

Now, considering the other contacts, it may be stated that T–T and R–R distances are directly related to the parameter a with the following relations:

$$d_{T-T} = a/\sqrt{2} \tag{7}$$

$$d_{R-R} = a \tag{8}$$

while the R–T contacts are related to the R–X contacts such that:

$$d_{R-T}^2 - d_{R-X}^2 = c^2/16 - d_{X-X}^2/4 - a^2/4 \tag{9}$$

Relationship (9) signifies that, in keeping d_{X-X} constant, an increase of the c/a ratio weakens the R–T contacts with respect to the R–X contacts.

From this preliminary review, it is shown that the main interatomic T–X, X–X and R–X contacts may be optimized by an interplay of a, c and z_{Ge} which, in turn, acts on the other T–T, R–T and R–R contacts.

In compounds involving strong T–X and X–X bonds, the system of Eqs. (4) to (6) may lead to a solution unrealistic for the other contacts. Hence, the

Table 1
Crystallographic data of the refined RT_2Ge_2 compounds

	a (Å)	c (Å)	V (Å^3)	c/a	z_{Ge}	B_R (Å^2)	B_T (Å^2)	B_{Ge} (Å^2)	R (%)	$N(I_o)$
$LaMn_2Ge_2$	4.1917(5)	10.965(1)	192.65	2.616	0.3809(2)	0.46(2)	0.61(4)	0.58(3)	5.8	173
$CaMn_2Ge_2$	4.1558(7)	10.857(2)	187.51	2.612	0.3835(1)	0.65(5)	0.64(3)	0.68(3)	6.7	148
UMn_2Ge_2	3.9877(6)	10.742(2)	170.82	2.694	0.3838(3)	0.46(3)	0.56(7)	0.54(6)	6.3	127
YFe_2Ge_2	3.9617(5)	10.421(1)	163.56	2.630	0.3789(3)	0.72(5)	0.93(4)	0.88(4)	7.2	112
$NdFe_2Ge_2$	4.0356(5)	10.490(1)	170.84	2.599	0.3752(1)	0.24(2)	0.38(2)	0.35(2)	3.2	179
$LaFe_2Ge_2$	4.1059(6)	10.562(1)	178.06	2.572	0.3719(2)	0.47(2)	0.69(4)	0.58(3)	6.4	155
YCo_2Ge_2	3.9698(4)	10.025(1)	157.99	2.525	0.3735(3)	0.51(4)	0.56(3)	0.59(3)	6.1	118
$NdCo_2Ge_2$	4.0371(4)	10.158(1)	165.56	2.516	0.3711(2)	0.55(2)	0.61(3)	0.59(2)	5.4	135
$LaCo_2Ge_2$	4.1030(4)	10.249(2)	175.54	2.498	0.3671(2)	0.10(2)	0.21(3)	0.18(3)	5.8	168
$CaCo_2Ge_2$	3.9900(5)	10.298(1)	163.94	2.581	0.3705(2)	0.58(5)	0.55(3)	0.56(3)	5.6	126
YNi_2Ge_2	4.0350(7)	9.757(2)	158.86	2.418	0.3720(2)	0.53(4)	0.69(3)	0.69(3)	5.1	114
$NdNi_2Ge_2$	4.1184(6)	9.824(1)	166.63	2.385	0.3697(2)	0.48(2)	0.85(3)	0.73(2)	3.6	140
$LaNi_2Ge_2$	4.1860(6)	9.902(1)	173.51	2.366	0.3667(2)	0.58(2)	0.88(4)	0.68(3)	6.8	165
$CaNi_2Ge_2$	4.0749(7)	9.987(2)	165.83	2.451	0.3697(1)	0.61(3)	0.73(2)	0.64(2)	3.1	147
$LaCu_2Ge_2$	4.2132(9)	10.161(2)	180.37	2.412	0.3752(2)	0.52(2)	0.95(4)	0.67(3)	6.0	153
$CaCu_2Ge_2$	4.1374(7)	10.221(1)	174.96	2.470	0.3793(2)	0.63(6)	0.95(4)	0.73(4)	6.8	100
$LaRu_2Ge_2$	4.2866(5)	10.121(1)	185.97	2.361	0.3653(2)	0.50(2)	0.45(2)	0.45(3)	4.9	149
$LaRh_2Ge_2$	4.174(1)	10.519(3)	183.26	2.520	0.3730(4)	0.56(4)	0.45(3)	0.62(6)	4.9	98
$LaPd_2Ge_2$	4.3669(5)	10.027(1)	191.21	2.296	0.3752(2)	0.50(2)	0.78(2)	0.72(2)	4.0	179
$LaMnCuGe_2$	4.2056(6)	10.596(1)	187.41	2.519	0.3774(4)	0.63(3)	1.05(5)	0.72(4)	5.7	97
$LaMnFeGe_2$	4.1375(4)	10.801(1)	184.90	2.611	0.3760(2)	0.43(2)	0.63(3)	0.59(2)	5.2	143
$CaFeMnGe_2$	4.0415(6)	10.830(2)	176.89	2.680	0.3811(2)	0.58(5)	0.67(3)	0.74(3)	5.8	152

observed interatomic distances will be a compromise between the main and minor contacts.

In systems without X–X bonds, optimized T–X and R–X contacts may be obtained through a wide range of a, c and z_{Ge} parameters and the results could account for one of the minor contacts.

The above remarks suggest that the strength of the various chemical bonds cannot be easily derived from the observed crystal data. It is, however, possible to extract some amount of information from the data, as will be proved in the following passages of this paper.

4.2. Variation of the cell parameters

The variations of the cell parameters $L = V^{1/3}$, a, c and c/a vs. the ionic radii of the R element (Ln^{3+} and/or Ca^{2+}) are presented in Figs. 3 and 4 [15]. Assuming linear variations of these parameters, a summary of the corresponding slopes is given in Table 5.

The calcium compounds fit the global variation of L quite well, except in the case of $CaMn_2Ge_2$. This anomaly might signify that the replacement of a

Table 2
Main interatomic distances and their corresponding relative dilatations in the RT_2Ge_2 (R = Y, Gd, Nd, La) compounds

Compound	d_{T-Ge} (Å)	Δ (%)	d_{Ge-Ge}	Δ (%)	d_{R-Ge}	Δ (%)	d_{T-T}	Δ (%)	d_{R-T}	Δ (%)	d_{R-R}	Δ (%)	Reference
YMn_2Ge_2	2.470(1)	−7.6	2.511(4)	−8.3	3.087(1)	−2.6	2.820(1)	+8.1	3.367(1)	+8.4	3.988(1)	+10.7	[8]
$NdMn_2Ge_2$	2.511(1)	−6.1	2.551(4)	−6.8	3.167(1)	−0.7	2.899(1)	+11.1	3.410(1)	+9.1	4.100(1)	+12.5	[8]
$LaMn_2Ge_2$	2.540(1)	−5.0	2.612(4)	−4.6	3.2389(9)	−0.2	2.9640(3)	+13.6	3.4507(3)	+8.5	4.1917(5)	+11.6	this work
YFe_2Ge_2	2.393(2)	−9.4	2.524(6)	−7.8	3.072(1)	−3.1	2.8013(3)	+9.9	3.2728(3)	+6.4	3.9617(5)	+10.0	this work
$NdFe_2Ge_2$	2.4076(6)	−8.9	2.618(2)	−4.4	3.1396(5)	−1.6	2.8536(3)	+12.0	3.3089(3)	+6.9	4.0356(5)	+10.8	this work
$LaFe_2Ge_2$	2.423(1)	−8.3	2.706(4)	−1.2	3.2031(9)	−1.3	2.9033(3)	+13.9	3.3447(3)	+6.1	4.1059(6)	+9.3	this work
YCo_2Ge_2	2.339(2)	−10.8	2.536(6)	−7.4	3.080(1)	−2.8	2.8071(2)	+12.1	3.1970(2)	+4.7	3.9698(4)	+10.2	this work
$NdCo_2Ge_2$	2.364(1)	−9.8	2.619(4)	−4.3	3.1406(9)	−1.5	2.8547(2)	+14.0	3.2440(2)	+5.6	4.0371(4)	+10.8	this work
$LaCo_2Ge_2$	2.377(1)	−9.3	2.724(4)	−0.5	3.2051(9)	−1.3	2.9013(2)	+15.9	3.2823(4)	+4.9	4.1030(4)	+9.3	this work
YNi_2Ge_2	2.342(1)	−10.4	2.498(4)	−8.8	3.1145(9)	−1.7	2.8532(3)	+14.4	3.1655(4)	+3.9	4.0350(7)	+12.0	this work
$NdNi_2Ge_2$	2.371(1)	−9.3	2.560(4)	−6.5	3.1811(8)	−0.3	2.9121(3)	+16.9	3.2050(3)	+4.5	4.1184(6)	+13.1	this work
$LaNi_2Ge_2$	2.391(1)	−8.6	2.640(4)	−3.6	3.2409(9)	−0.2	2.9599(3)	+18.8	3.2417(3)	+3.8	4.1860(6)	+11.5	this work
YCu_2Ge_2	2.425(2)	−8.4	2.431(6)	−11.2	3.094(2)	−2.4	2.845(1)	+11.3	3.263(1)	+5.3	4.024(2)	+11.7	[8]
$NdCu_2Ge_2$	2.444(2)	−7.7	2.478(8)	−9.5	3.168(2)	−0.7	2.915(1)	+14.0	3.280(1)	+5.8	4.123(2)	+13.2	[8]
$LaCu_2Ge_2$	2.461(1)	−7.0	2.536(4)	−7.4	3.2378(9)	−0.3	2.9792(5)	+16.6	3.3001(5)	+4.6	4.2132(9)	+12.2	this work
YRu_2Ge_2	2.423(3)	−10.5	2.53(1)	−7.7	3.241(2)	+2.2	2.985(1)	+11.5	3.236(1)	+3.1	4.221(1)	+17.2	[8]
$NdRu_2Ge_2$	2.431(1)	−10.2	2.627(4)	−4.0	3.281(1)	+2.8	3.006(1)	+12.2	3.278(1)	+3.7	4.252(1)	+16.7	[8]
$LaRu_2Ge_2$	2.440(1)	−9.9	2.727(4)	−0.4	3.3160(3)	+2.1	3.0311(3)	+13.2	3.3236(9)	+3.3	4.2866(5)	+14.2	this work
YRh_2Ge_2	2.428(1)	−10.5	2.481(5)	−9.4	3.148(1)	−0.7	2.894(1)	+7.6	3.268(2)	+3.9	4.092(1)	+13.6	[8]
$NdRh_2Ge_2$	2.450(1)	−9.7	2.573(4)	−6.0	3.195(1)	−0.2	2.925(1)	+8.7	3.322(1)	+4.9	4.136(1)	+13.6	[8]
$LaRh_2Ge_2$	2.455(2)	−9.5	2.672(8)	−2.4	3.240(2)	−0.2	2.9515(5)	+9.7	3.3573(7)	+4.2	4.174(1)	+11.1	this work
$GdPd_2Ge_2$	2.493(4)	−9.2	2.39(1)	−12.6	3.232(3)	+1.9	3.003(1)	+9.1	3.283(1)	+3.3	4.246(1)	+17.8	[8]
$NdPd_2Ge_2$	2.503(1)	−8.8	2.463(4)	−10.0	3.282(1)	+2.8	3.042(1)	+10.5	3.307(1)	+3.4	4.302(2)	+18.1	[8]
$LaPd_2Ge_2$	2.519(1)	−8.2	2.503(4)	−8.6	3.3245(3)	+2.4	3.0879(3)	+12.2	3.3318(8)	+2.4	4.3669(5)	+16.3	this work

Table 3
Comparison of the interatomic distances and their corresponding relative dilatations in the RT_2Ge_2 (R = Ca, Y, Nd, U) compounds

Compound	d_{T-Ge} (Å)	Δ (%)	d_{Ge-Ge}	Δ (%)	d_{T-T}	Δ (%)	d_{R-Ge}	d_{R-T}	d_{R-R}	Reference
YMn_2Ge_2	2.470(1)	−7.6	2.511(4)	−8.3	2.820(1)	+8.1	3.087(1)	3.367(1)	3.988(1)	[8]
UMn_2Ge_2	2.458(2)	−8.0	2.497(6)	−8.8	2.8197(3)	+8.1	3.084(1)	3.3456(4)	3.9877(6)	this work
$NdMn_2Ge_2$	2.511(1)	−6.1	2.551(4)	−6.8	2.899(1)	+11.1	3.167(1)	3.410(1)	4.100(1)	[8]
$CaMn_2Ge_2$	2.5335(7)	−5.2	2.530(2)	−7.6	2.9386(5)	+12.7	3.1992(5)	3.4183(5)	4.1558(7)	this work
$NdCo_2Ge_2$	2.364(1)	−9.8	2.619(4)	−4.3	2.8547(2)	+14.0	3.1406(9)	3.2440(2)	4.0371(4)	this work
$CaCo_2Ge_2$	2.349(1)	−10.4	2.667(4)	−2.6	2.8214(3)	+12.7	3.1207(9)	3.2570(3)	3.9900(5)	this work
$NdNi_2Ge_2$	2.371(1)	−9.3	2.560(4)	−6.5	2.9121(3)	+16.9	3.1811(8)	3.2050(3)	4.1184(6)	this work
$CaNi_2Ge_2$	2.3623(6)	−9.7	2.603(2)	−4.9	2.8814(4)	+15.6	3.1616(5)	3.2226(4)	4.0749(7)	this work
$NdCu_2Ge_2$	2.444(2)	−7.7	2.478(8)	−9.5	2.915(1)	+14.0	3.168(2)	3.280(1)	4.123(2)	[8]
$CaCu_2Ge_2$	2.455(1)	−7.2	2.467(4)	−9.9	2.9256(4)	+14.5	3.1751(9)	3.2877(3)	4.1374(7)	this work
$NdRu_2Ge_2$	2.431(1)	−10.2	2.627(4)	−4.0	3.006(1)	+12.2	3.281(1)	3.278(1)	4.252(1)	[8]
$CaRu_2Ge_2$	2.433(2)	−10.1	2.629(7)	−4.0	3.007(1)	+12.3	3.282(1)	3.281(1)	4.252(1)	[8]
$NdRh_2Ge_2$	2.450(1)	−9.7	2.573(4)	−6.0	2.925(1)	+8.7	3.195(1)	3.322(1)	4.136(1)	[8]
$CaRh_2Ge_2$	2.438(2)	−10.2	2.607(7)	−4.8	2.929(1)	+8.9	3.206(1)	3.316(1)	4.143(2)	[8]
$NdPd_2Ge_2$	2.503(1)	−8.8	2.463(4)	−10.0	3.042(1)	+10.5	3.282(1)	3.307(1)	4.302(2)	[8]
$CaPd_2Ge_2$	2.506(2)	−8.7	2.470(8)	−9.8	3.062(1)	+11.2	3.301(2)	3.305(1)	4.330(1)	[8]

Table 4
Evolution of the interatomic distances in the $RMn_{2-x}T_xGe_2$ (R = Ca, La; T = Fe, Cu) solid solutions

Compound	d_{T-Ge} (Å)	d_{Ge-Ge}	d_{R-Ge}	d_{T-T}	d_{R-T}	d_{R-R}
$LaMn_2Ge_2$	2.540(1)	2.612(4)	3.2389(9)	2.9640(3)	3.4507(3)	4.1917(5)
$LaMnFeGe_2$	2.476(1)	2.679(4)	3.2176(9)	2.9257(2)	3.4016(2)	4.1375(4)
$LaFe_2Ge_2$	2.423(1)	2.706(4)	3.2031(9)	2.9033(3)	3.3447(3)	4.1059(6)
$LaMn_2Fe_2$	2.540(1)	2.612(4)	3.2389(9)	2.9640(3)	3.4507(3)	4.1917(5)
$LaMnCuGe_2$	2.500(2)	2.592(8)	3.244(2)	2.9738(3)	3.3822(3)	4.2056(6)
$LaCu_2Ge_2$	2.461(1)	2.536(4)	3.2378(9)	2.9792(5)	3.3001(5)	4.2132(9)
$CaMn_2Ge_2$	2.5335(7)	2.530(2)	3.1992(5)	2.9386(5)	3.4183(5)	4.1558(7)
$CaMnFeGe_2$	2.470(1)	2.575(4)	3.1345(9)	2.8578(3)	3.3785(4)	4.0415(6)

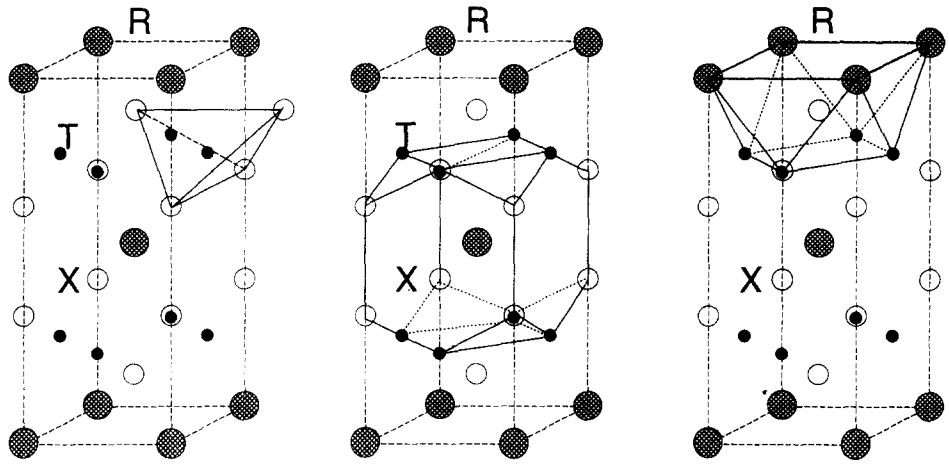

Fig. 1. Tridimensionnal representation of the RT_2X_2 ($ThCr_2Si_2$-type structure) showing the different coordination polyhedra: (a) tetrahedron around the T atoms; (b) 16-fold coordination polyhedron around the R atom; (c) metallic quadratic antiprism around the X atom.

lanthanide with calcium weakens chemical bonding in this compound. Other anomalies are systematically observed for the yttrium compounds: the tabulated ionic radius, $r_{Y^{3+}} = 0.892$ Å, seems to be too small [16]. Apparently, an intermediate radius of $r_{Y^{3+}} = 0.915$ Å, between that of Tb and Dy, seems to be more suitable.

The examination of the variation of L as a function of $r_{R^{3+}}$ and T provides useful information (Table 5). The large dL/dr slope of the manganese compounds suggests that the Mn–Ge sublattice, including the Mn–Ge, Ge–Ge and Mn–Mn contacts, is less tightly bound than the other T–Ge sublattices. According to corresponding slopes within the 3d series, the strength of

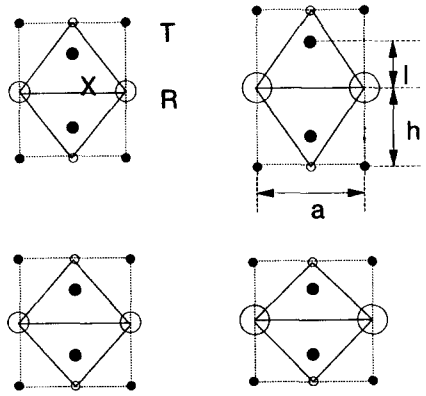

Fig. 2. Idealized deformations of the quadratic antiprisms to fit the increasing size of R: (top) *a* remains constant; (bottom) *l* remains constant.

the T–Ge sublattice increases from Fe to Cu. Moreover, the T–Ge sublattice comprising of 4d metals seems to be stronger.

The parameter *c* shows a negative variation, dc/dr, for the RCu_2Ge_2 series and practically no variation for the RPd_2Ge_2. According to previous remarks (see Section 4.1), this behaviour suggests strong Ge–Ge contacts in these compounds.

Lastly, the variation of the *c/a* ratio shows systematic anomalies for calcium compounds, with the exception of RCu_2Ge_2 series.

4.3. Variation of the interatomic distances in the rare earth compounds

The variation of interatomic distances are examined for yttrium (or gadolinium) and lanthanum compounds, i.e. compounds in which the largest variation of interatomic distances is expected. It is assumed that the variation of relative dilatation as a function of the size of the rare earth element ($d\Delta[i-j]/dr$) would be a better diagnostic than the absolute value of the relative dilatation. In such intermetallic compounds, an interatomic distance may be short owing to constraint by other interatomic contacts. However, when a bond is strong, one would expect very little variation in the presence of a larger R element which would tend to stretch the atomic framework.

The variation of the relative dilatation for T–X, X–X and T–T contacts, vs. the ionic radius of R, are presented in Figs. 5 to 7 and the corresponding slopes are gathered in Table 6. For yttrium, the cell parameters variation incited the use of the apparent ionic radius $r_{Y^{3+}} = 0.915$ Å as suggested by the cell parameters variations. The variations of the relative dilatation concerning the R–X and R–T contacts, vs. R size, are not significant as R element is probably in an ionic state and it is rather difficult to define the ionic radius of the counterion. Hence, we merely present a plot of the relative dilatation of the La–T and La–Ge contact for the various T elements (Fig. 8).

The Δ[T–Ge] values are strongly negative and their

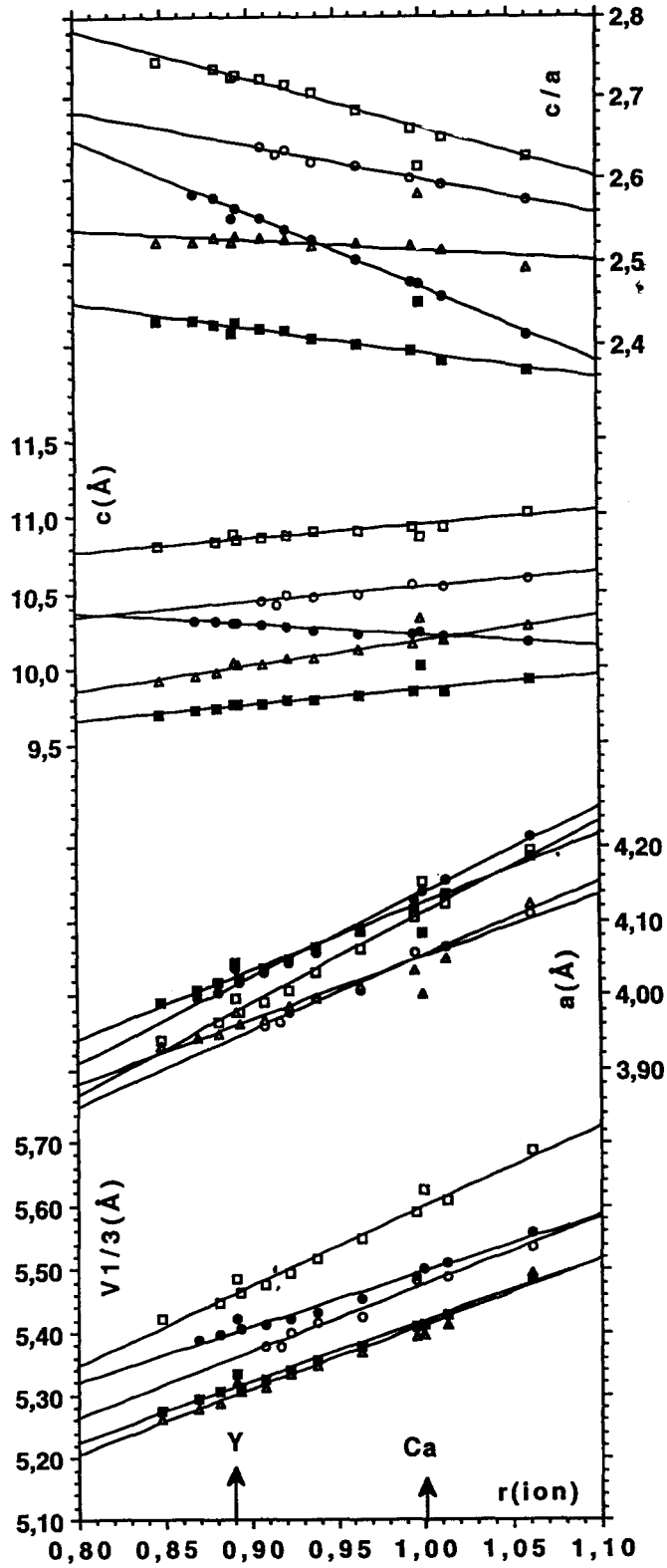

Fig. 3. R ionic radius dependence on the cell parameters of RT_2Ge_2 (R = Ca, Y, rare earths; T = 3d transition metals: □, Mn; ○, Fe; △, Co; ■, Ni; ●, Cu.

variation with the size of the rare earth element is weak, except for the Δ[Mn–Ge] value, which varies more strongly. This behaviour could be related to a weaker Mn–Ge bond. However, the Cu compounds are characterized by relatively weak values of Δ[Cu–Ge]; the variation of this value with the rare earth size is small.

The greatest variation is observed in the relative dilatation related to the Ge–Ge bond. The Cu and Pd compounds, characterized by strongly negative Δ[Ge–Ge] and rather weak variations of these values, are obviously separated from the other series. The Ge–Ge distances in Ni compounds are less contracted but the corresponding variation, $d(\Delta[Ge–Ge])/dr$, is rather small. The weakest variation of Δ[Ge–Ge] is observed in the Mn compounds. This behaviour could be related to the weakness of the Mn–Ge bond. It is further observed that, in Mn compounds, dilatation of the

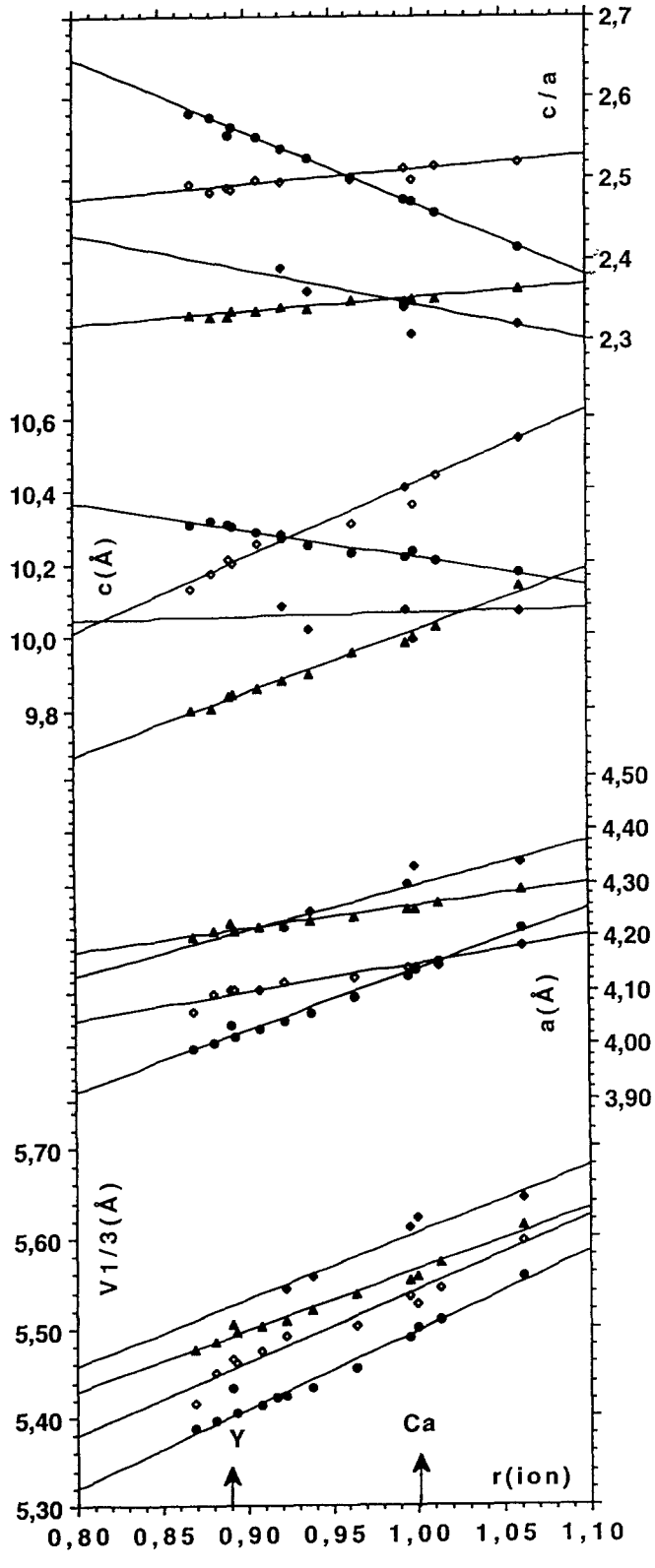

Fig. 4. R ionic radius dependence on the cell parameters of RT_2Ge_2 (R = Ca, Y, rare earths; T = 4d transition metals: ●, Cu; ▲, Ru; ◊, Rh; ♦, Pd.

Table 5
Variations of the cell parameters with the rare earth size (see Figs. 3 and 4)

T	dL/dr	da/dr	dc/dr	$d(c/a)/dr$
Mn	+1.26	+1.23	+0.89	−0.60
Fe	+1.07	+1.01	+0.96	−0.41
Co	+1.03	+0.85	+1.62	−0.13
Ni	+0.98	+0.92	+0.97	−0.31
Cu	+0.88	+1.16	−0.77	−0.89
Ru	+0.67	+0.42	+1.69	+0.16
Rh	+0.81	+0.51	+2.03	+0.18
Pd	+0.74	+0.83	+0.09	−0.44

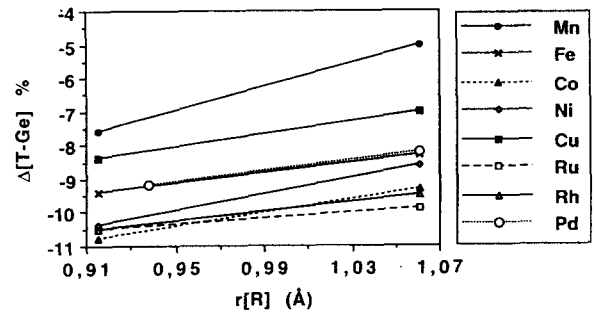

Fig. 5. Variation of the relative dilatation Δ[T–Ge] with the ionic size of the R element.

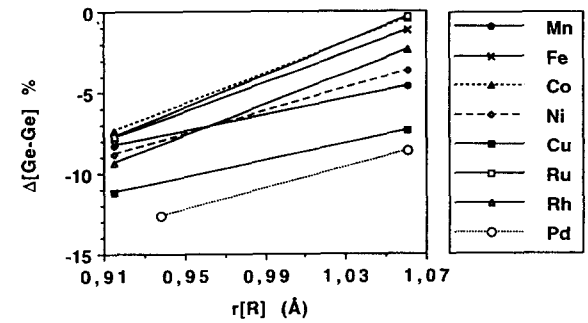

Fig. 6. Variation of the relative dilatation Δ[Ge–Ge] with the ionic size of the R element.

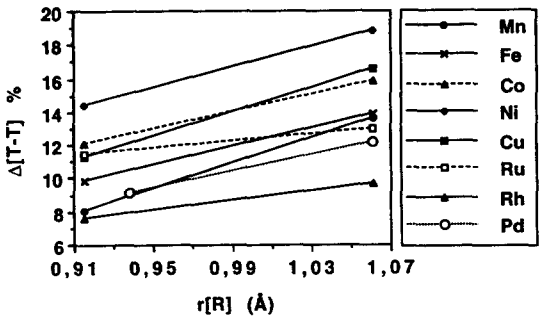

Fig. 7. Variation of the relative dilatation Δ[T–T] with the ionic size of the R element.

Table 6
Variation of the relative dilatations of the T–Ge, Ge–Ge and T–T contacts with the rare earth size for the various T metals (see Figs. 5 to 7)

Metal	dΔ(T–Ge)/dr	dΔ(Ge–Ge)/dr	dΔ(T–T)/dr
Mn	17.8	25.3	37.7
Fe	7.5	45.2	27.4
Co	10.3	47.3	26.0
Ni	12.3	35.6	30.1
Cu	9.6	26.0	36.3
Ru	4.1	50.0	10.3
Rh	6.8	47.9	14.4
Pd	8.1	32.5	25.2

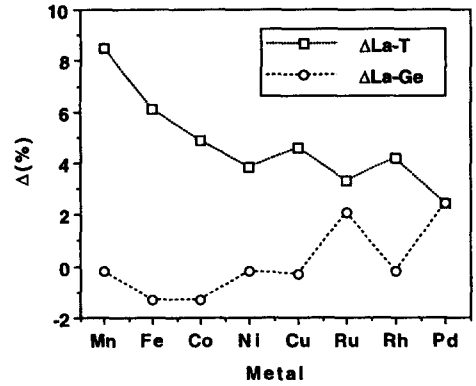

Fig. 8. Variation of the relative dilatations Δ[La–Ge] and Δ[La–T] as a function of the T metal.

(Mn,Ge) sublattice is mainly due to the d_{Mn-Ge} stretching.

The T–T distances are relatively large throughout the series with a homogeneous variation of Δ[T–T], except for Δ[Ru–Ru] and Δ[Rh–Rh], where a smaller variation is observed. This behaviour would suggest that, in compounds of the 4d series, the T–T contacts play an important role. The Pd compounds, however, behave differently. A strong variation of the parameter a is required to maintain the Ge–Ge bonds, as described in Section 4.1.

Δ[La–Ge] values are homogeneous except for Pd and Ru compounds. The behaviour of the Pd compounds is probably related to the relatively large size of the Pd atom. In these compounds, the Pd–Ge and Ge–Ge distances are probably close to their maximum contraction and the dimension of the (Pd,Ge) cage can no longer decrease. This could explain why the heaviest rare earth compounds cannot be synthesized. The behaviour of the Ru compounds is, in contrast, more intricate.

Excluding Mn and Fe compounds, the La–T contacts are rather homogeneous. The large corresponding interatomic distances should be related to the enthalpies of formation of the La–T compounds predicted by Miedema's model: positive values of ΔH are obtained for the Mn and Fe compounds [17].

Finally, we notice an inverted variation for Δ[La–Ge] compared with that of Δ[La–T]. Hence, it may be considered that an almost identical 16-fold coordination remains around the rare earth atom whatever the transition metal.

A summary of the interatomic contact dependences on the R size is given in Table 7. Accounting for the X–X, T–X and T–T contacts, four groups may be distinguished, (denoted as I, II, III and IV).

Group I (Mn) is characterized by a large variation of the Mn–Ge contacts, whereas variation of the Ge–Ge distances is the smallest of the studied compounds. According to the large variation of the cell volume with rare earth size, this fact would indicate a weakening of the Mn–Ge interaction rather than a strengthening of the Ge–Ge interaction. The large variation of the Mn–Mn contacts could be related to weak Mn–Ge contacts since both bonds are mainly directed along the a axis.

Group II (Cu, Pd, Ni) is characterized by small variations in Ge–Ge and T–Ge contacts. According to Section 4.1, the small variations in Ge–Ge and T–Ge contacts with R size yields large variations of the a parameter and, consequently, of T–T distances.

Group III (Fe, Co) and IV (Rh, Ru) are both characterized by a large variation of Ge–Ge contacts and a small variation in T–Ge contacts. They are, however, distinguished by the evolution of T–T con-

Table 7
Summary and classification of the variations of d(Δ[$i-j$])/dr related to the contacts X–X, T–X and T–T

		X–X		T–X		T–T	
I	Mn	25.3	Small	17.8	Large	37.7	Large
II	Cu	26.0	Small	9.6	Small	36.8	Large
	Pd	32.5		8.1		25.2	
	Ni	35.6		12.3		30.1	
III	Fe	45.2	Large	7.5	Small	27.4	Large
	Co	47.3		10.3		26.0	
IV	Rh	47.9	Large	6.8	Small	14.4	Small
	Ru	50.0		4.1		10.3	

tacts. According to Section 4.1, the absence of strong Ge–Ge contacts allows an interplay of minor interactions. Group IV is obviously characterized by small variations in T–T contacts. The RRu_2Ge_2 and RRh_2Ge_2 series behave quite similarly to the RRu_2P_2 series, characterized by an absence of variation in Ru–P and Ru–Ru contacts. The Ge–T_2–Ge slab remains almost unchanged throughout the rare earth series. If T–T contacts intervene, it is worth noting that their equilibrium distance is not identical in both series; d_{Ru-Ru} ranges around 3.0 Å, while d_{Rh-Rh} ranges around 2.92 Å, in spite of their similar elemental radii. It is also remarkable that the Ru–Ru distances are approximately identical in the RRuGe related compounds (d_{Ru-Ru}(LaRuGe) = 3.036 Å and d_{Ru-Ru}(NdRuGe) = 3.017 Å) [18].

4.4. Variation of the interatomic distances with the valence of the R element

The variation of Δ[T–Ge] and Δ[Ge–Ge] for Nd and Ca compounds are plotted in Fig. 9. In several compounds, the Δ[T–Ge] and Δ[Ge–Ge] values are insensitive to the valence change, i.e. as in the case of Cu, Ru and Pd compounds. In Co, Ni and Rh compounds, characterized by relatively weak Ge–Ge contacts, substitution of Nd by Ca further weakens the corresponding bonds. Consequently, and in maintaining the T–Ge polyhedra around the R element, the T–Ge distances decrease. In Mn compounds this situation is inverted. Here, the Mn–Ge bond is relatively weak and substitution of Nd by Ca further weakens it.

Synthesis of the $CaFe_2Ge_2$ compound was unsuccessful. According to variations observed in $CaNi_2Ge_2$ and $CaCo_2Ge_2$, it may be assumed that the Ge–Ge bond is even weaker in $CaFe_2Ge_2$. The non-existence of this compound could be related to this effect.

Lastly, it is observed that the substitution of Y by U

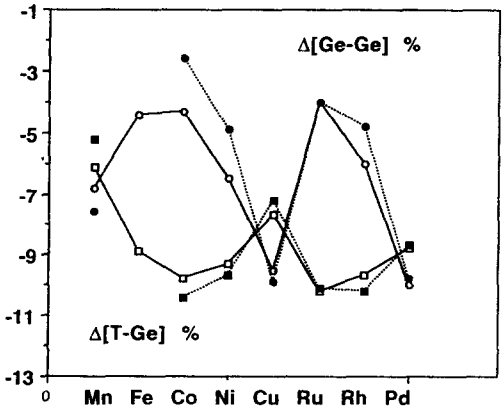

Fig. 9. Effect of the substitution of Nd by Ca on the relative dilatations Δ[Ge–Ge] and Δ[T–Ge] as a function of the T metal: squares, Δ[T–Ge]; circles, Δ[Ge–Ge]; open symbols, Nd; full symbols, Ca.

(probably in the 4+ valence state) induces a slight contraction of the Mn–Ge and Ge–Ge bonds (Table 3).

4.5. Variation of the interatomic distances in several $RMn_{2-x}T_xGe_2$ solid solutions (R = Ca, La; T = Fe, Cu)

The refinement of $LaMnFeGe_2$ and $LaMnCuGe_2$ shows a continuous near linear variation of the mean interatomic distances. A fair approximation of the interatomic distances in the solid solutions may be obtained by linear interpolation.

The study of $CaMnFeGe_2$ shows that the substitution of manganese by iron yields a significant increase of the Ge–Ge interatomic distance. The non-stable $CaFe_2Ge_2$ compound is probably characterized by large Ge–Ge distances as in $CaNi_2Ge_2$ and $CaCo_2Ge_2$.

5. Conclusions

The single crystal X-ray diffraction study of ternary germanides RT_2Ge_2 provides new information on the evolution of chemical bonding in $ThCr_2Si_2$-type structure compounds.

The results may be compared with conclusions of previous theoretical work on isotypic RMn_2P_2 phosphides [19]. According to Hoffmann et al., the Fermi level sinks as one moves to the right-hand side of the Periodic Table. Thus, on the left of the transition series, the metal Fermi level is above the P–P σ^*, both σ and σ^* are occupied and there is no resultant P–P bond.

The study of the d_{Ge-Ge} variations obviously enables us to distinguish two groups of Ge–Ge contacts as a function of the transition metal. If Mn compounds are excluded, our results agree quite well with calculations carried out by Hoffmann and Zheng calculations; i.e. in moving to the right-hand side of the Periodic Table, strong Ge–Ge contacts are observed in Ni, Cu and Pd compounds.

The particular behaviour of Mn compounds could be related to the relative weakness of the Mn–Ge bond. In this case, the stretching of the Mn–Ge cage is mainly accommodated by an expansion of the Mn–Ge bonds. Such assumption is corroborated by the cell volume dependence on the R size which is considerably stronger than in the other compounds.

The absence of strong Ge–Ge contacts in the other transition metal (Fe, Co, Ru, Rh) compounds permits an interplay of other interactions such as R–T, R–R and T–T. The variations of the corresponding interatomic distances suggest an important role of the T–T contacts in Ru and Rh compounds in which the Ge–T_2–Ge slab remains almost unchanged throughout the rare earth series.

Among the remaining Fe and Co compounds, it is rather difficult to distinguish the contact which controls cell parameters and z_{Ge} coordinate. The relatively large R–T distances suggest a weak affinity between the rare earth and Mn, Fe and perhaps even Co.

In view of these results, we must now question the Mn magnetic behaviour.

In previous work, it has been suggested that the magnetic behaviour of the Mn planes may be related to the relative strengths of a ferromagnetic Mn–Mn direct exchange and a negative Mn–Ge–Mn superexchange, and thus, related to the Mn–Mn and Mn–Ge distances [20]. The plot of the molecular field constant $N_1 = (T_N - \theta_p)/2C$ vs. the ratio $r = d[\text{Mn–Mn}]/[d[\text{Mn–Ge}]$ corresponding to the compounds $LaMn_2Ge_2$ [20], $CaMn_2Ge_2$ [7], $LaMnCuGe_2$ and $LaMnFeGe_2$ [6], given in Fig. 10, does not show any obvious correlation between both parameters. This probably suggests that more complicated phenomena are involved.

One of the main results of this crystallographic study is the great variability of the Mn–Ge bond. Hence, the Mn–Ge overlapping and the filling of the 3d shell, should greatly vary with rare earth size. The considerable range of the Mn moment value, from approximately 2 μ_B in heavy rare earth compounds [2] to approximately 3 μ_B in $LaMn_2Ge_2$ [3] is probably a result of this effect. The sign of the exchange integrals might also be inverted along the rare earth series. For a given R ionic radius, it has been shown that the substitution of Nd by Ca considerably weakens the Mn–Ge bond. Hence, the drastic change of the magnetic properties from $NdMn_2Ge_2$ to $CaMn_2Ge_2$ might also be related to this effect.

The substituting 3d metals carry a more complicated role as the substitution modifies both the strength of the interatomic contacts and also the filling of the 3d shells. Moreover, the effect of the substitution may be different depending on whether it acts on a compound within which the Mn–Ge bond is stretched or contracted.

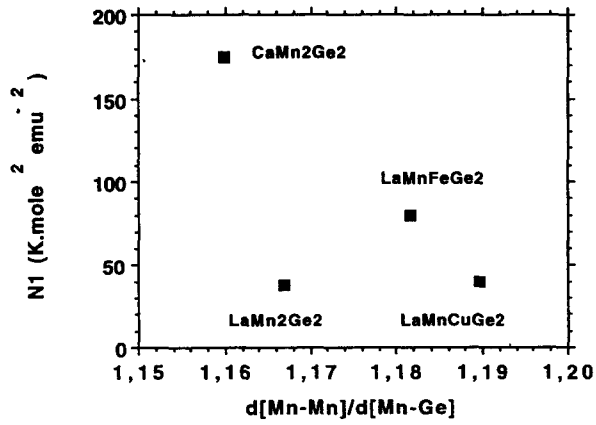

Fig. 10. Correlation between the ratio d_{Mn-Mn}/d_{Mn-Ge} and the mean field coefficient N_1.

The present work enables us to predict the interatomic distances in the solid solutions studied here. The study of the magnetic properties of other solid solutions involving different T and R metals should permit a better understanding of the underlying phenomenons. According to the c/a variations observed at the F–AF transition in $SmMn_2Ge_2$ [21], it would be interesting to re-examine the interatomic distances in each magnetic state by single crystal refinement. The different c/a radii should induce slight variations in the various contacts. It would also be interesting to further examine the Mn compounds in their paramagnetic state in order to detect any change of the interatomic distances at the ordering point.

References

[1] Z. Ban and M. Sikirica, *Acta Crystallogr., 18* (1965) 594.
[2] A. Szytula and J. Leciejewicz, Magnetic properties of ternary intermetallic compounds of the RT_2X_2 type, in K.A. Gschneider, Jr. and L. Eyring (eds.), *Handbook on the Physics and Chemistry of Rare Earths*, Vol. 12, Elsevier, Amsterdam, 1989, Chapter 83, p. 133.
[3] G. Venturini, R. Welter, E. Ressouche and B. Malaman, *J. Alloys Comp., 210* (1994) 213.
[4] B. Malaman, G. Venturini, R. Welter and E. Ressouche, *J. Alloys Comp., 210* (1994) 209.
[5] G. Venturini, R. Welter, E. Ressouche and B. Malaman, *J. Alloys Comp., 224* (1995) 262.
[6] M.N. Norlidah, personal communication, 1995.
[7] R. Welter, personal communication, 1995.
[8] G. Venturini, B. Malaman and B. Roques, *J. Solid State Chem., 79* (1989) 136.
[9] G.M. Sheldrick, *Program for Crystal Structure Determination*, 1976 (University of Cambridge, UK).
[10] B. Eisenmann, N. May, W. Müller, H. Schäfer, A. Weiss, J. Winter and G. Ziegleder, *Z. Naturforsch. Teil B:, 25* (1970) 1350.
[11] W. Dörrscheidt, N. Niess and H. Schäfer, *Z. Naturforsch. Teil B:, 31* (1976) 890.
[12] E. Teatum, K. Gschneider and J. Waber, in W.B. Pearson (ed.), *The Crystal Chemistry and Physics of Metals and Alloys*, Wiley, New York, 1972, p. 151
[13] W. Jeitschko, R. Glaum and L. Boonk, *J. Solid State Chem., 69* (1987) 93.
[14] R. Madar, personal communication, 1988.
[15] P. Villars and L.D. Calvert, *Pearson's Handbook of Crystallographic Data for Intermetallic Phases*, American Society for Metals, Materials Park, OH, 1991, 2nd edn.
[16] R.D. Shannon and C.T. Prewitt, *Acta Crystallogr. Sect. B:, 25* (1969) 925.
[17] A.R. Miedema, *J. Less-Common Met., 46* (1976) 67.
[18] R. Welter, G. Venturini, B. Malaman and E. Ressouche, *J. Alloys Comp., 202* (1993) 165.
[19] R. Hoffmann and C. Zheng, *J. Phys. Chem., 89* (1985) 4175.
[20] G. Venturini, *J. Alloys Comp.*, in press.
[21] E.M. Gyorgy, B. Batlogg, J.P. Remeika, R.B. van Dover, R.M. Fleming, H.E. Blair, G.P. Espinosa, A.S. Cooper and R.G. Maines, *J. Appl. Phys., 61* (1987) 4237.